

9. Materials and methods are available as supporting material on Science Online.
 10. R. Polishchuk, A. Di Pentima, J. Lippencott-Schwartz, *Nat. Cell Biol.* **6**, 297 (2004).
 11. R. K. Tweten, in *Virulence Mechanisms of Bacterial Pathogens*, J. A. Roth et al., Eds. (American Society for Microbiology, Washington, DC, 1995), pp. 207–230.
 12. J. M. Gaullier, E. Ronning, D. J. Gilloly, H. Stenmark, *J. Biol. Chem.* **275**, 24595 (2000).
 13. H. M. Schrager, J. G. Rheinwald, M. R. Wessels, *J. Clin. Invest.* **98**, 1954 (1996).
 14. C. Cywes, M. R. Wessels, *Nature* **414**, 648 (2001).
 15. P. Nyberg et al., *EMBO J.* **23**, 2166 (2004).
 16. D. H. Walker, V. L. Popov, P. A. Crocquet-Valdes, C. J. Welsh, H. M. Feng, *Lab. Invest.* **76**, 129 (1997).
 17. K. A. Rich, C. Burkett, P. Webster, *Cell. Microbiol.* **5**, 455 (2003).
 18. B. R. Dorn, W. A. Dunn, A. Progulsk-Fox, *Infect. Immun.* **69**, 5698 (2001).
 19. J. Pizarro-Cerda, E. Moreno, V. Sanguedolce, J. L. Mege, J. P. Gorvel, *Infect. Immun.* **66**, 2387 (1998).
 20. S. Sturgill-Koszycki, M. S. Swanson, *J. Exp. Med.* **192**, 1261 (2000).
 21. K. Kirkegaard, M. P. Taylor, W. T. Jackson, *Nat. Rev. Microbiol.* **2**, 301 (2004).
 22. We thank M. Yaffe for providing 3xFYVE-EGFP plasmid. We also thank T. Tokuhisa, M. Hatano, and A. Kuma for generating the wild-type and *Atg5^{-/-}* MEF cell lines. This work was supported in part by Grants-in-Aid and 21st Century Center of Excellence

(COE) program at Osaka University Graduate School of Dentistry from the Ministry of Education, Culture, Sports, Science and Technology in Japan.

Supporting Online Material

www.sciencemag.org/cgi/content/full/306/5698/1037/DC1

Materials and Methods

Figs. S1 to S4

References

Movie S1

12 August 2004; accepted 4 October 2004

Structural Insights into the Assembly of the Type III Secretion Needle Complex

Thomas C. Marlovits,^{1,2} Tomoko Kubori,² Anand Sukhan,^{2*} Dennis R. Thomas,³ Jorge E. Galán,² Vinzenz M. Unger^{1†}

Type III secretion systems (TTSSs) mediate translocation of virulence factors into host cells. We report the 17-angstrom resolution structures of a central component of *Salmonella typhimurium* TTSS, the needle complex, and its assembly precursor, the bacterial envelope–anchored base. Both the base and the fully assembled needle complex adopted multiple oligomeric states in vivo, and needle assembly was accompanied by recruitment of the protein PrgJ as a structural component of the base. Moreover, conformational changes during needle assembly created scaffolds for anchoring both PrgJ and the needle substructure and may provide the basis for substrate-specificity switching during type III secretion.

Type III secretion systems (TTSSs) are central to the virulence of many Gram-negative bacteria pathogenic for animals and plants (1, 2). In addition to the needle complex (3), which is the core component of these systems, TTSSs are composed of more than 20 proteins, including a highly conserved group of integral membrane proteins, a family of customized cytoplasmic chaperones, and several accessory proteins (1, 2), placing TTSSs among the most complex protein secretion systems known. In *S. typhimurium*, the needle complex is formed by a base and a filamentous needle, composed of a single protein, PrgI, that projects ~50 nm from the bacterial surface (Fig. 1, A and B) (3). The base is formed by InvG, PrgH, and PrgK (4) and features four distinct rings, two associated with the outer membrane (OR1 and OR2 in Fig. 1A) and another

two that are in close proximity to the inner membrane (IR1 and IR2 in Fig. 1A). The entire complex is essential for virulence (5)

and is believed to provide a conduit for the direct transport of proteins from the bacterial cytoplasm to the host cell. Here, we have used electron cryomicroscopy to visualize the detailed structural organization of the *S. typhimurium* needle complex, as well as structural changes that occur during the last step of its assembly.

Quantitative amino acid analysis revealed that the components of the base, InvG: PrgH:PrgK, were present in 1:1:1 molar ratios [fig. S1 (6)], suggesting that the three proteins were structurally linked by a shared rotational symmetry. Our attempts to determine this symmetry by labeling the base with antibodies or gold, as well as by scanning transmission electron microscopy analysis, all yielded ambiguous results (7). Moreover, the resolution in several reconstructions stalled at ~30 Å despite increasing the number of particle images in the data sets. This suggested sample heterogeneity. To test whether the heterogeneity was caused by different rotational symmetries, we used a

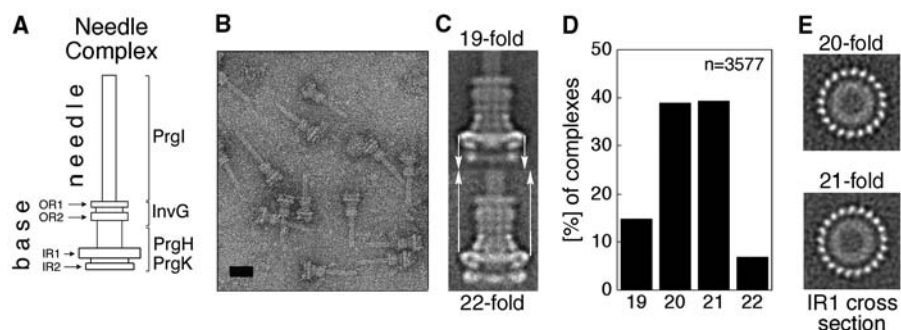


Fig. 1. The needle complex and the base complex of the TTSS from *S. typhimurium* can adopt different symmetries in vivo. (A) Nomenclature of the structural features of the needle complex. The needle complex is divided into two distinctive substructures: the membrane-embedded base and the extracellular needle filament. The base spans the periplasm and is associated with the inner and outer membranes, where ringlike structures are visible in electron micrographs of negatively stained needle complexes (2% phosphotungstic acid, pH 7) (B). The outer membrane-associated rings (OR1 and OR2) are composed of the protein InvG, and the inner membrane-associated rings (IR1 and IR2) contain the proteins PrgH and PrgK (4). The only protein identified for the needle filament to date is PrgI (4). Bar, 30 nm. (C) Model-based multireference alignment revealed significant differences in the diameters of the average projections obtained for different rotational symmetries, as indicated by white arrows in the comparison of the IR1 of the 19- and 22-fold particles. (D) Distribution of different symmetries in needle complexes isolated from wild-type *S. typhimurium*. The data were generated by examining 3577 particles. (E) After sorting of the particles and 3D reconstruction without enforcing any symmetry, the true rotational symmetries could be derived from cross sections through IR1 of the reconstructed needle complexes, as shown for the 20- and 21-fold particles.

¹Department of Molecular Biophysics and Biochemistry, Yale University School of Medicine, New Haven, CT 06520–8024, USA. ²Section of Microbial Pathogenesis, Yale University School of Medicine, New Haven, CT 06536, USA. ³Rosenstiel Basic Medical Sciences Research Center, Brandeis University, Waltham, MA 02454, USA.

*Present address: Department of Microbiology, Oklahoma State University, Stillwater, OK 74078, USA.

†To whom correspondence should be addressed. E-mail: vinzenz.unger@yale.edu

supervised classification procedure by constructing a multireference data set for image alignment (6). As reported for other single-particle specimens (8, 9), this strategy improved resolution and resolved the data sets for the base and the entire needle complex into subpopulations of particles with different and well-defined symmetries (Fig. 1, C to E). Specifically, complexes with 20- and 21-fold rotational symmetry (-fold) were the most abundant species, accounting for about 40% of the total number of particles each (Fig. 1D). Whether the differently sized complexes serve different physiological pur-

poses or reflect a functionally silent polymorphism remains unclear.

Sorting of the images into symmetry classes enabled us to reconstruct three-dimensional (3D) structures for the 20- and 21-fold bases and needle complexes. Final density maps were filtered to 17 Å resolution based on the 0.143 Fourier Shell Correlation criterion (6). The base appeared as a cylindrical structure, 300 Å tall and 240 Å wide, that could be divided into two distinct substructures localized to the outer and inner membranes (Fig. 2, A and B). In surface renderings, only the IR rings showed

a division into distinct subunits, whereas the OR rings appeared mostly featureless (Fig. 2, A and B; movie S1). This difference most likely was due to the predicted high content of β structure in InvG, and the fact that the smaller diameter of the OR rings, compared to the IR rings (Fig. 3C), caused subunit spacing to be at or below the resolution limit.

Overall, the structures of the base and needle complex appeared similar (Fig. 2, A and B), yet tilted views of their volumes revealed notable differences. Both the base and needle complex showed a cuplike protrusion, which extended from the center of a basal plate that is part of IR1. This protrusion was larger in the needle complex (Fig. 2B) than in the base (Fig. 2A) and may serve as a point of entry for proteins that are to be secreted and/or may serve as a docking site for the export apparatus, which was absent in our samples. At its apical side, the base was closed by a septum (Fig. 2A), most likely formed by a domain of InvG, whereas in the needle complex, a filamentous needle protruded from the base projecting outward from the cell surface (Fig. 2B). Cropping of the reconstruction revealed that the base was hollow inside (Fig. 2C). Bounded by the septum at its apical side, the internal chamber was closed by a continuous plate at its basal side. A socketlike structure extended into the hollow chamber from the basal plate (Figs. 2C and 3A) and served as an anchor for the channel (referred to as “inner rod”) that, in the needle complex, traversed the chamber of the base (Fig. 3A). Notably, the socket may also function as an adaptor that coupled the N-fold IR1 to the inner rod, whose symmetry is likely to be different from the symmetry of the base.

Contoured longitudinal sections revealed conformational changes that occurred during the transition from the base to the fully assembled needle complex (Fig. 3, A and B). The cuplike protrusion that emerged from the basal plate of IR1 moved down, while an inward, clamping movement of IR2 redefined the shape of the cavity that is located below the basal plate of the base (movie S2). These conformational changes may provide the structural basis for the functional reprogramming of the TTSS machinery, which upon completion of needle assembly, switches from secreting the needle protein PrgI, the inner-rod protein PrgJ (see below), and the regulatory protein InvJ (4, 10–13) to secreting the effector proteins that are delivered into the host cell (12, 14). On the opposite side of the basal plate, the socketlike structure underwent an outward movement, which created an attachment point for the inner rod (movie S2). A similar outward movement was observed for OR1, which created space for the needle to dock at the outermost perimeter of the

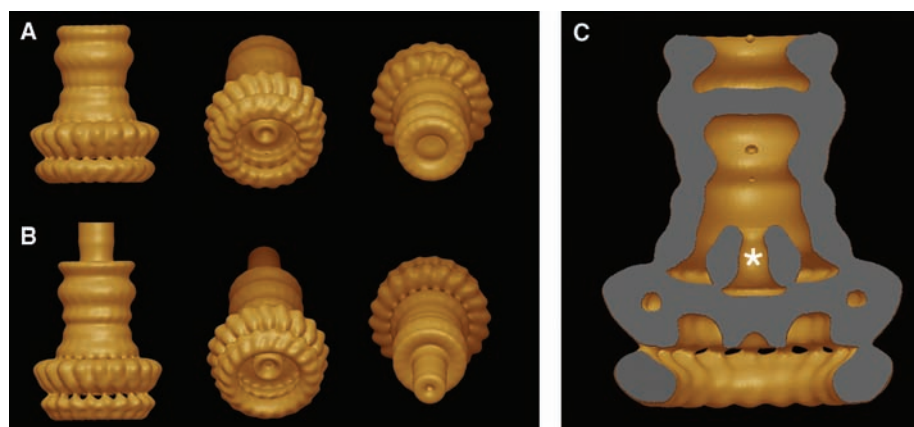


Fig. 2. Surface renderings of the structures of the base (A) and the needle complex (B) show individual subunits within the IR rings, but the OR rings appear smooth. The structure shown here is that of the 20-fold complex with 20-fold symmetry imposed. The absolute hand of the reconstruction was not determined. (A) The contouring threshold represents $\sim 120\%$ of the expected mass of the 20-fold base (2.69 MDa), assuming a protein density of $0.844 \text{ dalton}/\text{\AA}^3$ (IMAGIC-5, Image Science Software GmbH, Germany) and including a 13% contribution of the detergent bound to the two membrane-embedded regions of the complex. Owing to the uncertainty in the number of PrgI and PrgJ subunits present in the final reconstruction of the needle complex (B), the clearly defined subunits of IR1 of the base were used as a point of reference for thresholding of the needle complex because this part of IR1 is largely unaffected by the conformational changes during needle assembly and, hence, should closely match the appearance in the base (movie S2). Structural differences between the base and needle complex are described in the text. (C) Removal of the front half of the base shows its internal chamber. A socketlike structure, marked by an asterisk, extends into the chamber's interior and serves as an anchoring point for the “inner rod” in the needle complex.

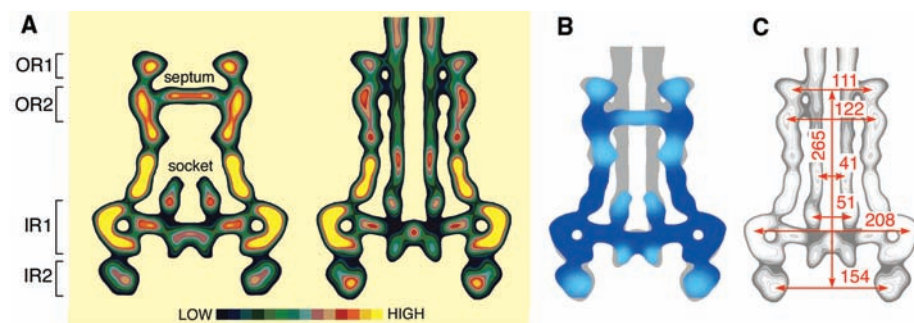
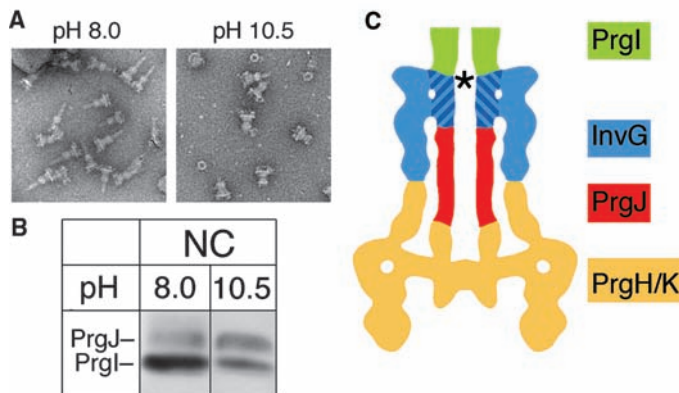


Fig. 3. Needle assembly induces large conformational changes in the base. (A) Contoured longitudinal sections show the distribution of protein density within the base and needle complexes. Protein densities are represented by 14 evenly spaced contour levels starting at 1 σ above the mean densities of the volumes. (B) An overlay of the longitudinal sections for the base (blue) and needle complex (gray) reveals regions of high conformational flexibility (light blue). (C) Key dimensions of the needle complex, given in Å, were measured from center to center because such measurements are independent of contouring thresholds and increments.

Fig. 4. PrgJ is recruited as a structural component to the base during needle assembly. (A) Electron micrographs of needle complexes before (pH 8.0) and after subsection to pH 10.5 to affect needle disassembly. (B) Western blot analysis of untreated and pH 10.5-treated needle showed that elevated pH drastically diminished the amount of the needle protein PrgI, as expected based on the images shown in (A), but did not affect the amount of PrgJ, which, therefore, must be located within the base. (C) Model cartoon summarizing the proposed organization of the five major structural components of the needle complex: PrgH, PrgK, PrgJ, InvG, and PrgI. Hatched coloring indicates the uncertainty in the exact boundaries of PrgI, InvG, and PrgJ. The asterisk marks the location where the secretion tunnel markedly narrows at the entry point to the needle, which attaches to the outermost periphery of the base through a contact with InvG.



base (movie S2). These changes were complemented by an outward movement of OR2 and a drastic remodeling that flattened the septum, sealing the apical side of the base, against OR2 during needle assembly (Fig. 3, A and B; movie S2). This rearrangement of the septum is essential for creation of the secretion channel and transformed part of InvG from being a barrier into forming two scaffolds that enable assembly of the needle and the inner rod. Like the socket structure at the basal end of the chamber, these new scaffolds likely serve as adaptors, accommodating the symmetry mismatches between the base, the needle, and the inner rod.

The diameter of the secretion channel narrowed at the outermost boundary of the base before opening to the central channel of the needle substructure (Figs. 3A and 4C). This change of diameter could not be reconciled with the helical symmetry of the filamentous needle, formed by PrgI, and suggested that the rod inside the base was formed by another protein. The most likely candidate to form the inner rod was PrgJ, which has been detected in needle-complex preparations (10, 13). To test this hypothesis, we subjected purified needle complexes to an elevated pH. This treatment caused disassembly of the needle filament (Fig. 4A), yet did not affect the amount of PrgJ (Fig. 4B), which therefore must be localized within the base. Moreover, quantitative amino acid analysis revealed that in needle complexes, PrgJ and PrgI were present in 1:6 molar ratios (fig. S3), which was too high to support previous models suggesting that PrgJ exclusively caps the tip of the needle (13, 15) [such a ratio should be at least 1:24 (6)].

Our structural analysis of the needle complex of the *S. typhimurium* TTSS revealed that the needle attaches to the base

at its outermost periphery and identified a new substructure formed by InvG and PrgJ. Moreover, visualization of conformational changes that contribute to reprogramming of TTSS to secrete effector proteins provides essential insights into structure-function relationships of this important virulence factor.

References and Notes

- G. R. Cornelis, F. Van Gijsegem, *Annu. Rev. Microbiol.* **54**, 735 (2000).
- J. E. Galán, A. Collmer, *Science* **284**, 1322 (1999).
- T. Kubori *et al.*, *Science* **280**, 602 (1998).
- T. Kubori, A. Sukhan, S. I. Aizawa, J. E. Galán, *Proc. Natl. Acad. Sci. U.S.A.* **97**, 10225 (2000).

- J. E. Galán, R. Curtiss III, *Proc. Natl. Acad. Sci. U.S.A.* **86**, 6383 (1989).
- Materials and methods are available as supporting material on Science Online.
- T. C. Marlovits, T. Kubori, J. E. Galán, V. Unger, unpublished results.
- M. Valle *et al.*, *EMBO J.* **21**, 3557 (2002).
- S. Yang *et al.*, *J. Mol. Biol.* **321**, 839 (2002).
- A. Sukhan, T. Kubori, J. E. Galán, *J. Bacteriol.* **185**, 3480 (2003).
- C. Collazo, J. E. Galán, *Infect. Immun.* **64**, 3524 (1996).
- A. Sukhan, T. Kubori, J. Wilson, J. E. Galán, *J. Bacteriol.* **183**, 1159 (2001).
- T. G. Kimbrough, S. I. Miller, *Proc. Natl. Acad. Sci. U.S.A.* **97**, 11008 (2000).
- J. E. Galán, *Annu. Rev. Cell Dev. Biol.* **17**, 53 (2001).
- A. Blocker *et al.*, *Mol. Microbiol.* **39**, 652 (2001).
- We thank D. J. DeRosier and F. Sigworth for helpful discussions about the image processing. We are grateful to the Yale School of Medicine for the support of the Cryo Electron Microscopy Core Facility; N. Grigorieff (Brandeis University) for the use of a computer cluster; and the Howard Hughes Medical Institute Keck Facility at Yale for the quantitative amino acid analysis. Molecular graphics images (Fig. 2) were produced using the UCSF Chimera package from the Computer Graphics Laboratory, University of California, San Francisco (NIH P42 RR-01081). This work was supported by Public Health Service grants GM35433 from the NIH to D. J. DeRosier (supporting D.R.T), AI30492 to J.E.G., and GM66145 to V.M.U. and by a Hellman Family Fellowship to V.M.U. The structure of the Needle Complex has been deposited in the EmDep Database with accession code EMD-1100.

Supporting Online Material

www.sciencemag.org/cgi/content/full/306/5698/1040/DC1
 Materials and Methods
 Figs. S1 to S3
 References
 Movies S1 and S2

12 July 2004; accepted 3 September 2004

Tracking SNARE Complex Formation in Live Endocrine Cells

Seong J. An and Wolfhard Almers*

Syntaxin, synaptosome-associated protein of 25 kD (SNAP25), and vesicle-associated membrane protein/synaptobrevin are collectively called SNARE receptor (SNARE) proteins, and they catalyze neuronal exocytosis by forming a "core complex." The steps in core complex formation are unknown. Here, we monitored SNARE complex formation in vivo with the use of a fluorescent version of SNAP25. In PC12 cells, we found evidence for a syntaxin-SNAP25 complex that formed with high affinity, required only the amino-terminal SNARE motif of SNAP25, tolerated a mutation that blocks formation of other syntaxin-SNAP25 complexes, and assembled reversibly when Ca²⁺ entered cells during depolarization. The complex may represent a precursor to the core complex formed during a Ca²⁺-dependent priming step of exocytosis.

The fusion of secretory vesicles with the plasma membrane is essential for the release of transmitters from neurons and of hormones from endocrine cells. It is catalyzed by the combination of syntaxin (Syx) and SNAP25 on the plasma membrane with vesicle-associated membrane protein/synaptobrevin (Syb) on vesicles. The three proteins, collectively called SNAREs, assemble into an

exocytic core complex that pulls membranes close together (1) by forming a twisted bundle of four parallel α helices (2). In this coiled coil, one helix is formed by Syx, another by Syb, and one each by the two SNARE motifs of SNAP25. The core complex almost certainly forms in steps. Indeed, partial SNARE complexes can form in solution (3), but it is unclear which of them, if any, are core